

<https://doi.org/10.1038/s44183-024-00064-8>

# Electrochemical ocean iron fertilization and alkalinity enhancement approach toward CO<sub>2</sub> sequestration

Check for updates

Amir Taqieddin<sup>1</sup>, Stephanie Sarrouf<sup>2</sup>, Muhammad Fahad Ehsan<sup>2</sup>, Ken Buesseler<sup>3</sup> & Akram N. Alshwabkeh<sup>2</sup>✉

Achieving net-zero emissions by 2050 requires the development of effective negative emission techniques, including ocean-based approaches for CO<sub>2</sub> sequestration. However, the implementation and testing of marine CO<sub>2</sub> removal (mCDR) techniques such as ocean iron fertilization (OIF) or ocean alkalinity enhancement (OAE) face significant challenges. Herein, a novel self-operating electrochemical technology is presented that not only combines OIF and OAE, but also recovers hydrogen gas (H<sub>2</sub>) from seawater, hence offering a promising solution for achieving quantifiable and transparent large-scale mCDR. Experimental results show that the electrochemical OIF (EOIF) can not only increase the concentration of ferrous iron (Fe<sup>+2</sup>) by 0–0.5 mg/L, but also significantly increases the seawater pH by 8% (i.e., a 25% decrease in the hydrogen ions concentration). The release of iron (Fe<sup>+2</sup>/Fe<sup>+3</sup>) can be regulated by adjusting the magnitude of the electric current and its form (e.g., pulsed current and polarity reversal), as well as by optimizing the electrode material and geometry. In certain ocean regions, enhanced iron concentrations stimulate the naturally occurring biological carbon pump (BCP), leading to increased phytoplankton growth, CO<sub>2</sub> uptake, and subsequent export of carbon to the deep ocean. Simultaneously, the system increases seawater alkalinity and the buffer capacity, enhancing CO<sub>2</sub> solubility and storage in the shallow ocean through the solubility pump. The obtained measurements demonstrate the scalability of EOIF and its ability to operate using solar energy at a lower cost. Overall, the proposed EOIF technology offers a practical, effective, and sustainable solution for addressing climate change on a large scale.

The severe environmental and human health consequences of continuous anthropogenic greenhouse gas emissions require effective and novel solutions. The catastrophic results of climate change, such as the rise in wildfires, floods, and ecosystem disruptions<sup>1–4</sup> highlight the critical need of urgent and innovative global-scale solutions for carbon dioxide removal (CDR). A target has been set by the United Nations Framework Convention on Climate Change to achieve net-zero emissions by 2050<sup>5–7</sup>, which requires mitigating ~800 Gt carbon dioxide (CO<sub>2</sub>) by 2050<sup>8</sup>. This means that we are required to find possible solutions for avoiding these cumulative emissions of CO<sub>2</sub> through adapting reduced emission technologies, utilizing effective carbon capture and removal approaches. In fact, achieving net-zero will require not only reducing emissions, but also removing tens of Gt CO<sub>2</sub> from

the atmosphere annually. This scale of removal exceeds the capability of any single existing CDR technology. Relying only in conventional emission reduction techniques, such as transitioning to clean energy technologies (e.g., renewable energy, electric vehicles)<sup>9–16</sup> will not be sufficient to achieve the 2050 target<sup>5–7</sup>. The development and implementation of net-negative emissions technologies (NET) that are designed to remove CO<sub>2</sub> directly from the atmosphere and sequester carbon (C) in the ocean for 100 s to 1000 years<sup>17–19</sup>, such as marine CDR (mCDR)<sup>20,21</sup>, are crucial toward achieving the goal of net-zero emissions.

CDR is defined as intervention actions that remove CO<sub>2</sub> from the atmosphere<sup>22</sup>. Designing efficient and cost-effective CDR methods has been one of the primary goals in tackling climate change issues due to their

<sup>1</sup>Department of Mechanical & Industrial Engineering, Northeastern University, Boston, MA 02115, USA. <sup>2</sup>Department of Civil & Environmental Engineering, Northeastern University, Boston, MA 02115, USA. <sup>3</sup>Woods Hole Oceanographic Institution, Marine Chemistry and Geochemistry Department, 266 Woods Hole Rd., Woods Hole, MA 02543, USA. ✉e-mail: [a.alshwabkeh@northeastern.edu](mailto:a.alshwabkeh@northeastern.edu)

potential to remove a large amount of atmospheric CO<sub>2</sub>. These methods rely on using nature-based technologies for CDR via preserving Earth's nature and ecosystems<sup>23</sup>. For example, the amount of organic carbon that can be sequestered in soil from the atmosphere is potentially between 0.79 and 1.54 Gt/year<sup>24</sup>. This approach requires the implementation of sustainable land and soil management protocols to design natural CDR solutions<sup>25</sup>. Enhancing rock weathering could deliver a net CDR of 6–30 Mt<sub>CO<sub>2</sub></sub>/year as one natural carbon sequestration solution based on the modeling studies<sup>26</sup>. This accelerated weathering approach could uptake 45% of the atmospheric CDR for the United Kingdom to achieve its 2050 net-zero emissions target. Alternatively, ocean-based CDR methods are considered promising climate solutions since the ocean can be viewed as a large sink for sequestering the anthropogenic CO<sub>2</sub> (i.e., up to 30% of CO<sub>2</sub> emitted by human activities)<sup>20,27</sup>. In terms of capacity, the ocean can store 50 times the amount of CO<sub>2</sub> present in the atmosphere and 10–20 times more than all plants and soil<sup>24,28</sup>.

mCDR techniques are divided into two main categories: abiotic and biotic methods. Ocean alkalinity enhancement (OAE) is an abiotic approach that is focused on increasing the alkalinity of the seawater to increase the buffer capacity of the ocean and enhance air-sea gas exchange via the solubility pump<sup>29–33</sup>. Generally, increasing the pH of seawater increases the saturation state for carbonate minerals<sup>34</sup>, which are used by many marine organisms to form shells and skeletons depending on several factors (e.g., temperature, salinity)<sup>29–31</sup>. As increased levels of CO<sub>2</sub> enter the ocean and react with water, forming carbonic acid and decreasing ocean pH, OAE would cause additional atmospheric CO<sub>2</sub> removal to counter the deleterious impact of ocean acidification. A modeling study conducted in the Bering Sea demonstrated that the mCDR efficiency could increase to 96% after three years of total alkalinity enhancement<sup>33</sup>. On the other hand, ocean iron fertilization (OIF) is a biotic approach for mCDR in which iron (Fe) is supplied<sup>35,36</sup> as an essential micronutrient in certain areas of the ocean where it limits primary production (see Fig. 1a). Therefore, even small amounts of Fe can greatly stimulate the net growth of phytoplankton<sup>7,35–45</sup>. As the phytoplankton population expands and photosynthesis increases, dissolved CO<sub>2</sub> in the ocean decreases, and the uptake of atmospheric CO<sub>2</sub> increases<sup>46,47</sup>. Through a biological carbon pump (BCP), the organic C derived from sinking heterotrophs creates organic-rich “marine snow” particles that sink, exporting 3% of the organic C down to the deep ocean and sea floor, where it would be sequestered for hundreds to thousands of years<sup>48,49</sup>. Several field experiments and studies have shown the promising potential of increasing mCDR using OIF, suggesting that the ocean could sequester gigatons of additional atmospheric CO<sub>2</sub><sup>7,38,41,44,50–53</sup> if OIF were applied to large areas of the ocean that have high macronutrients (such as nitrate and phosphate) and low Fe. For example, enhanced carbon export into the deep water has been achieved by field experiments of natural iron fertilization at the Southern Ocean<sup>54</sup>. The significant potential of OIF as a large-scale negative emission technology and natural CDR solution has recently brought substantial attention from the scientific community and policymakers to advancing OIF techniques<sup>7,17,21,36,50</sup>.

While both OIF and OAE represent promising mCDR solutions, testing and the implementation of these two approaches have been challenging. For example, regulating and monitoring the Fe release in the ocean through repeated additions over a long term is arduous<sup>7,43,55</sup>. The main advantage of OIF as an mCDR approach is that the Fe concentrations needed to stimulate phytoplankton growth are low compared to other nutrients. In natural systems, the Fe:C ratio in marine phytoplankton is 1:100,000 or even less (i.e., less Fe)<sup>56</sup>, making this one of the most cost-effective mCDR approaches. Traditional OIF methods operate by releasing bulk quantities of Fe in the ocean via ships/airplanes as solid particles or in aqueous form (see Fig. 1a)<sup>36,43</sup>. Prior experiments have shown that most of the added Fe through FeSO<sub>4</sub> is lost due to rapid oxidation, precipitation, and scavenging by sinking particles, and/or is considered not readily bioavailable<sup>55</sup>. Additionally, the requirement of having a ship on site, or possible delivery by aircraft for the Fe release limits the supply to shorter-term additions. However, for mCDR deployments, longer-term and

repeated Fe additions over larger areas may be more effective. Increasing the bioavailability of the supplied iron over time and through repeated deployment to the phytoplankton requires a clear understanding of the iron speciation (e.g., ferrous versus ferric)<sup>57</sup>. While ferrous (Fe<sup>+2</sup>) is more soluble in seawater than ferric (Fe<sup>+3</sup>), both forms can be taken up by marine phytoplankton<sup>39</sup>. The bioavailability and the uptake of these species by phytoplankton depend on the reductive thermodynamic processes and seawater conditions (see Sutak et al. -2020 for more details<sup>39</sup>). It is important to note that Fe<sup>+3</sup> is predominant in oxygenated and neutral pH surface waters since Fe<sup>+2</sup> is oxidized under these conditions. Larger concentrations of Fe<sup>+2</sup> can be formed as the pH decreases (i.e., more acidic) compared to Fe<sup>+3</sup><sup>58</sup>. Understanding the interdependent relationship between the iron speciation, oxygen content, and pH level is crucial for enhancing iron bioavailability.

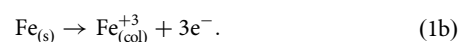
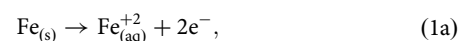
Several electrochemical techniques have been developed and proposed as mCDR solutions<sup>59–64</sup>. These techniques are mainly designed to increase the alkalinity of seawater to capture CO<sub>2</sub><sup>59–64</sup>. For instance, an earlier study demonstrated the potential of using electrochemical systems that convert CO<sub>2</sub> into calcium carbonate by inducing local changes in the pH at the cathode<sup>63</sup>. Recently, an electrochemical system comprising of bismuth and silver electrodes was tested to capture and release chloride ions from seawater, leading to changes in the overall pH through CO<sub>2</sub> removal<sup>59</sup>. These proposed electrochemical systems use inert anodes, which produce acids or chlorine gas (Cl<sub>2</sub>) during electrolysis leading to unfavorable conditions (e.g., a decrease in the pH of seawater) at the anode. Further, these systems use inert metal as anode and cathode, such as bismuth and silver, which makes scaling expensive. Finally, the previously developed electrochemical systems<sup>59–64</sup> tend to rely only on OAE as a mitigation strategy for mCDR without realizing the promising potential of OIF.

Motivated by utilizing ocean-based CDR solutions to tackle climate change at a global scale, a novel EOIF approach is proposed that combines OIF and OAE to improve the ocean capacity for carbon storage and CDR sequestration. Our approach to advancing these systems as mCDR solution is focused on employing Fe/Fe-producing anodes to eliminate the production of acids at the anode in traditional electrochemical OAE systems and replace it with Fe release<sup>65–68</sup>. In this case, the electrochemical system implements both OIF and OAE techniques at the anode and cathode, respectively, where the cathode can be made from naturally abundant cost-effective materials, such as carbon. The proposed EOIF approach overcomes major limitations of the existing electrochemical techniques for mCDR. The design and the concept of the proposed EOIF technology are discussed. Experimental evidence on its ability to regulate the Fe release in seawater and increase the pH is discussed. Additionally, the EOIF system is designed to extract H<sub>2</sub> from the seawater as detailed in the following section. Overall, the EOIF represents a promising sustainable, self-operating, and effective solution for mCDR.

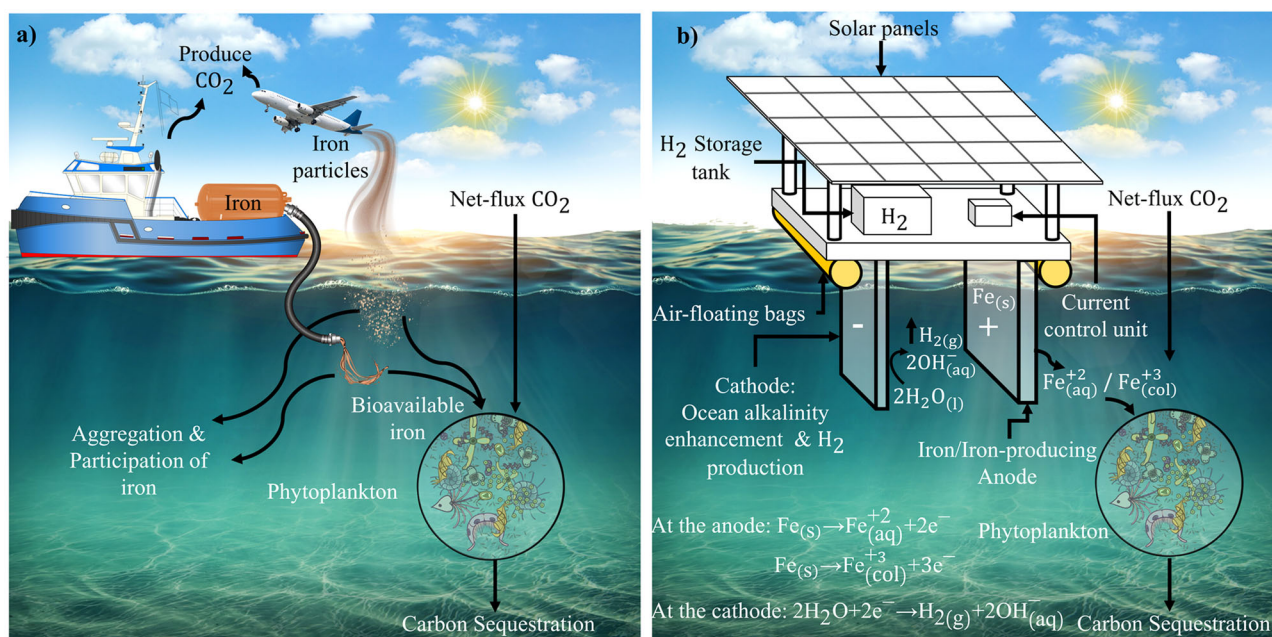
## Results

### EOIF technology

The proposed EOIF relies on releasing Fe in the ocean *via* electrochemical reactions at the electrode as shown in Fig. 1b. When an electrical current is applied across the electrodes, ferrous ions, Fe<sup>+2</sup>, will be directly released in aqueous phase from a solid Fe/Fe-producing anode<sup>65,69,70</sup>. The ferric ions, Fe<sup>+3</sup>, can be released in a colloidal form. The electrochemical reactions of Fe<sup>+2</sup> and Fe<sup>+3</sup> at the anode have standard potential reactions equal to 0.44 V and 0.037 V, respectively, and given as<sup>58</sup>:



The main advantage of the EOIF technology is its ability to regulate and control the release of Fe according to Faraday's law where the amount of



C)

Traditional OIF Methods	EOIF Technology
<ul style="list-style-type: none"> <li>• Fe is supplied <i>via</i> an airplane or a ship which operates on fossil-fuel</li> <li>• Fe is released in seawater as an aqueous or solid particles which are mixed with other chemicals</li> <li>• Large amount of the supplied Fe precipitate due to the limited control/regulation of Fe release over time</li> <li>• These methods require close monitoring</li> <li>• Supplying Fe is limited to short term additions</li> <li>• The OIF system size is limited to the airplane/ship capability</li> <li>• Traditional OIF methods could be expensive since it requires pre-preparation of Fe and it involves several logistics</li> </ul>	<ul style="list-style-type: none"> <li>• Fe is supplied <i>via</i> an electrochemical system which can be powered by solar energy</li> <li>• Fe is directly released in seawater as an aqueous or a colloidal form maximizing its bioavailability</li> <li>• The electrochemical Fe released is coupled with OAE <i>via</i> OH<sup>-</sup> generation at the cathode</li> <li>• The processes are precisely controlled through tuning the applied electrical current</li> <li>• The EOIF system can be designed as a mobile and self-operating platform</li> <li>• The platform can recover H<sub>2</sub> gas from the ocean in addition to both the OIF and OAE processes</li> <li>• The EOIF system allows multiple additions of Fe over long term as needed</li> <li>• The EOIF system is scalable and can be deployed as several small platforms to cover multiple regions or as a large single platform to cover on region</li> <li>• The EOIF system is cost-effective solution with less logistics compared to traditional OIF methods</li> </ul>

**Fig. 1 | Schematic of OIF approaches.** **a** traditional OIF using boat or airplane to release Fe in seawater in pre-prepared aqueous or solid particles forms, **b** the proposed EOIF technology, which is envisioned as a mobile offshore platform that is powered by solar energy panels, and **c** summary of the benefits of EOIF compared to traditional methods.

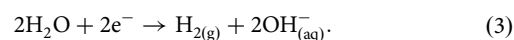
released Fe (*m*) is given as:

$$m = \frac{I \times t \times M_w}{n \times F} \quad (2)$$

where *I* is the electrical current, *t* is the duration of the reaction, *M<sub>w</sub>* is the molecular mass of the Fe, *n* is the number of participating electrons, and *F* is Faraday’s constant. Clearly, *m* can be directly controlled by tuning the values of *I* and *t*. In this manner, the flux of Fe in the ocean can be controlled over time and space to maximize the bioavailability and distribution of Fe in the ocean and avoid any oversupply leading to Fe saturation in the ecosystem which could lead to precipitation of siderite or eutrophication style effects.

Further, the reactions at the cathode can also be designed to boost and enhance the alkalinity of the ocean. At the cathode, seawater splitting takes

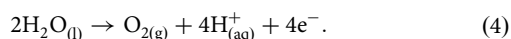
place as follows:



The produced H<sub>2</sub> can be collected and recovered for later usage as fuel such as powering the EOIF system. More importantly, the released OH<sup>-</sup> in the ocean will increase the ocean’s alkalinity without the need to add additional minerals to seawater. The enhanced alkalinity and pH will help increase the ocean’s capacity to intake atmospheric CO<sub>2</sub> and de-acidify the ecosystem. The cathode material selection is not limited to a specific choice if it ensures optimized chemical reaction kinetics. For example, the cathode material can be made of carbon as a cost-effective choice<sup>71,72</sup>. Here, several cathode materials were tested. The Fe and OH<sup>-</sup> generated in-situ from the electrodes transfer directly into the seawater in their dissolved aqueous form,

eliminating the need for additional chemicals (e.g.,  $\text{SO}_4^{2-}$  in case of  $\text{FeSO}_4$  additions). Specifically, the proposed OAE approach does not generate unnecessary acid components during alkalinity enhancement, unlike traditional OAE approaches<sup>33</sup>.

It should be noted that secondary competing reactions can take place at electrode surfaces which can lower the efficiency of the EOIF system. For example, depending on the system pH, hydrolysis or oxidation of  $\text{Fe}_{(\text{aq})}^{+2}$  can lead to the formation of either aqueous ferric ( $\text{Fe}_{(\text{aq})}^{+3}$ ) or ferrous hydroxide ( $\text{Fe}(\text{OH})_{2(\text{s})}$ ) precipitates<sup>58,73</sup>. Chloride ions can also react at the anode to form chlorine gas or are adsorbed at the anode by the surface polarization<sup>74,75</sup>. Additionally, oxygen evolution reaction (OER) can also occur at the anode as follows:



The generated  $\text{O}_2$  gas can be collected and stored or can end up leaving the ocean's surface in the atmosphere. In general, Fe oxidation is typically the dominant reaction at the anode. Furthermore, the electrical current can be adjusted to prevent other competing reactions. At the cathode, secondary reactions can also occur such as converting the formed  $\text{OH}^-$  to  $\text{O}_2$  gas. Therefore, it is important to control the environment of the reactions to reduce unnecessary secondary reactions at the electrodes.

Overall, the EOIF system can be deployed as a mobile offshore platform, as shown in Fig. 1b. The key features of the EOIF platform are summarized in Fig. 2. Produced gases, such as  $\text{H}_2$ , are considered as secondary products (refer to Fig. 2). A key innovation of the EOIF is its ability to control the rate of Fe release according to Faraday's law where the release flux is directly proportional to the current at the electrodes. The system can be self-operating in offshore environments, which lowers the total cost and carbon footprint compared to traditional OIF methods that require a ship or an airplane for operations (Fig. 1a). Further, it represents a cost-effective solution given it has a simple design that combines both OIF and OAE concepts for tackling climate change.

### Electrochemical iron release in seawater

Various experiments were performed to demonstrate and verify the release of Fe in seawater using EOIF. First, the release of  $\text{Fe}^{+2}$  and  $\text{Fe}^{+3}$  was investigated in artificial seawater, deionized (DI) water, and natural seawater. The natural seawater was collected from the shore labs at Woods Hole Oceanographic Institute, as indicated in the method sections. These specific experiments were performed in 1 L beakers where Fe plates were used as both anode and cathode. The current in this set of experiments was set to 160 mA. Figure 3 shows the concentration of  $\text{Fe}^{+2}$  and  $\text{Fe}^{+3}$  in artificial, DI,

and natural raw (i.e., unfiltered) seawater as a function of time. Although the concentration profiles are nonlinear due to the exchange between different chemical forms of Fe (i.e.,  $\text{Fe}^{+2}$  and  $\text{Fe}^{+3}$ )<sup>65,69</sup>, an increase in the Fe concentrations was observed as a function of time due to electrochemical processes. Specifically, the initial concentrations of both  $\text{Fe}^{+2}$  and  $\text{Fe}^{+3}$  in the artificial seawater are zero since it was prepared using DI water without any iron traces. Immediately after 5 min of applying the electrical current and initiating the electrochemical reactions (i.e., first collected data point in all experiments), the presence of different forms of Fe ( $\text{Fe}^{+2}/\text{Fe}^{+3}$ ) was observed in both artificial and DI seawater samples.

The Fe concentration ranges are within the typically measured range of released Fe in natural waters<sup>66-78</sup>. It should be noted that the iron concentration in the ocean is on the scale  $\sim 5.6 \times 10^{-5}$  mg/L (or 1 nmol/L). The obtained measurements indicate a maximum value of  $\sim 0.5$  mg/L of  $\text{Fe}^{+2}$  in raw seawater (Fig. 3a), and  $\sim 1$  mg/L of  $\text{Fe}^{+3}$  in artificial seawater, as shown in Fig. 3b. This value can be lowered by decreasing the current intensity. Here, a relatively large current was applied to ensure the released Fe is within the detection limit of the measuring instrument. More important, the tests were performed in 1 L systems. In the actual ocean, the volume of water will be significantly larger, and the concentration of Fe will thus be more diluted for the same released amount of Fe where it can be expected to reach the target range of  $\sim 5.6 \times 10^{-5}$  mg/L. Figure 3a initially shows a decrease in  $\text{Fe}^{+2}$  concentration in raw seawater due to an increased  $\text{Fe}^{+3}$  concentration (as shown in Fig. 3b). However, the  $\text{Fe}^{+2}$  concentration subsequently increases after the concentration of  $\text{Fe}^{+3}$  is stabilized.

The amount of  $\text{Fe}^{+2}$  concentration in the reactor increases almost linearly as a function of time during 30–100 min of the reaction. However, the  $\text{Fe}^{+3}$  concentration decreases between 30–60 min and increases again between 60 and 150 min. The decrease in the concentration of  $\text{Fe}^{+3}$  indicates the transformation of  $\text{Fe}^{+3}$  to  $\text{Fe}^{+2}$  between 30–60 min. After 60 min, the concentration of  $\text{Fe}^{+2}$  becomes large enough, and, therefore, part of the  $\text{Fe}^{+2}$  is transformed into  $\text{Fe}^{+3}$ . While the presence of  $\text{Fe}^{+3}$  is essential to assist in absorbing  $\text{Fe}^{+2}$  by phytoplankton<sup>39,79</sup>, it is important to keep it under control since it displays low solubility in the water at near neutral pH. Our results show that the electrochemical approach can offer the potential to optimize the  $\text{Fe}^{+3}$  concentration as a function of time in seawater (i.e., specifically a minimum concentration of  $\text{Fe}^{+3}$  at time 60 min in raw seawater experiment). Figure 3 shows that the ratio of  $\text{Fe}^{+3}$  to  $\text{Fe}^{+2}$  concentration is about 0.65 at 150 min of the electrochemical reaction in the raw seawater sample (i.e.,  $\text{Fe}^{+3}$  and  $\text{Fe}^{+2}$  concentrations are about 0.3 and 0.45 mg/L, respectively). This means that  $\text{Fe}^{+2}$  concentration is about 60% of the total released Fe in raw seawater sample at 150 min. At 60 min, the ratio of concentration is about 0.15 indicating an optimized reaction time at which the released  $\text{Fe}^{+2}$

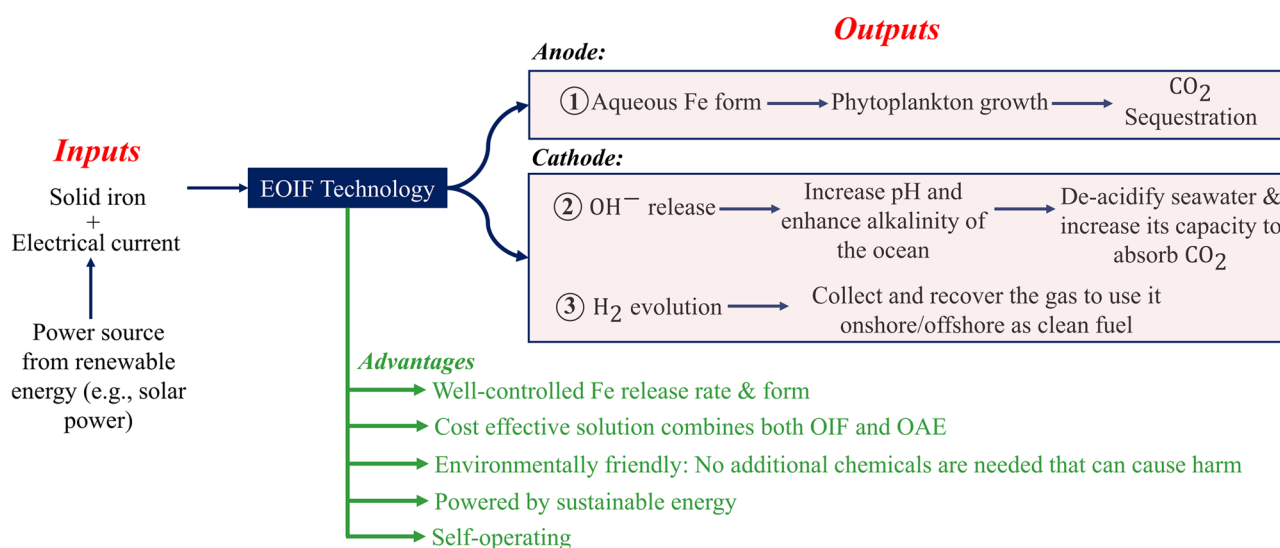
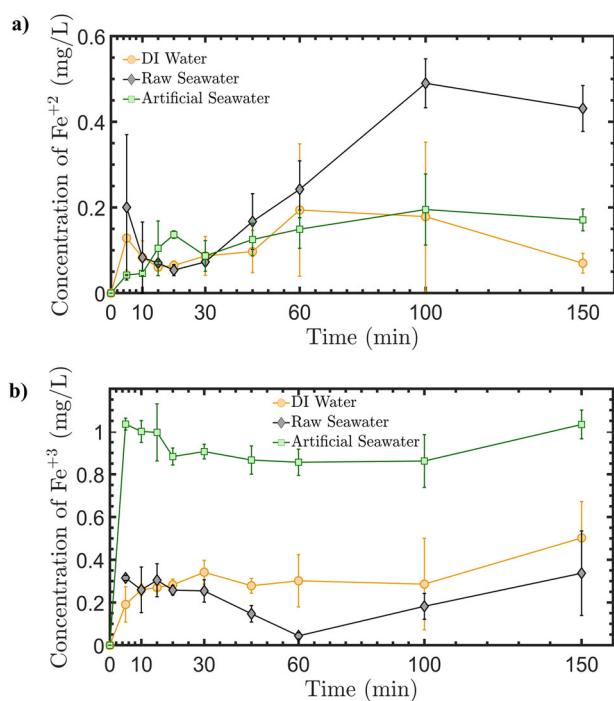


Fig. 2 | Summary of the EOIF technology. Schematic of the inputs, outputs and advantages.



**Fig. 3 | Measured concentrations of the electrochemically released iron as a function of time in various water samples and under 160 mA electrical current. a Fe<sup>2+</sup> and b Fe<sup>3+</sup> concentrations.**

is maximized compared to Fe<sup>3+</sup> (i.e., Fe<sup>3+</sup> and Fe<sup>2+</sup> concentrations are about 0.036 and 0.24 mg/L, respectively) where the concentration of Fe<sup>2+</sup> is about 87% of the total released Fe in the raw seawater sample. This suggests that the electrochemical reactions for releasing Fe can be controlled and stopped at a specific time once optimized conditions are achieved. In other words, the amount and the chemical nature of the released Fe can be controlled over time to maximize the bioavailability of the generated Fe by the electrodes.

Lower Fe<sup>2+</sup> and higher Fe<sup>3+</sup> concentrations were observed in artificial seawater and DI water. For DI water, a low total amount of Fe is released due to its low ionic conductivity as an electrolyte compared to artificial and raw seawater which is rich with various ions. The low ionic conductivity reduces the efficiency of the Faradaic reactions leading to lower Fe flux from the electrodes. Demonstrating the electrochemical Fe release in DI water establishes a control experiment base to further investigate the effect of adding minerals for the synthesis of artificial seawater. Two different chemical compositions of artificial seawater were tested (see Table S1). The electrochemical release of Fe in both composition samples shows the same concentration of Fe<sup>2+</sup> and Fe<sup>3+</sup> as a function of time (see Figure S3). The presence of biological species and complex chemical compounds in raw seawater assist in keeping the electrochemically released Fe in solution, leading to higher Fe<sup>2+</sup> and significantly lower Fe<sup>3+</sup> concentrations compared to the artificial seawater. This is confirmed by running the electrochemical experiments under the same conditions using filtered and UV oxidized seawater (i.e., UV and 100 µm filtered samples). The results (see Figure S4) show that lower Fe<sup>2+</sup> concentrations are detected in filtered seawater samples toward the end of the experiments. Thus, a larger concentration of insoluble Fe<sup>3+</sup> is observed in artificial seawater due to the absence of natural organic matter compared to raw natural seawater, which is important to the solubility of released Fe. Specifically, Fig. 3 illustrates that the concentrations of Fe<sup>3+</sup> in artificial seawater are approximately three times higher than that in the raw natural seawater sample, while the Fe<sup>2+</sup> concentration is approximately two times lower. In the following sections, various approaches were investigated to control electrochemical Fe release in artificial seawater, including manipulating the ratio of Fe<sup>3+</sup> to Fe<sup>2+</sup> concentrations. It should be highlighted that the expected concentration of Fe<sup>3+</sup> and Fe<sup>2+</sup> in

natural seawater is significantly less and larger, respectively, compared to the artificial seawater results based on the results in Fig. 3 and the previous discussion. In the following sections, the experiments focus on investigating Fe production in artificial seawater, allowing more experimental control given their chemistry rather than natural raw seawater.

### Regulating electrochemical iron release

According to Eq. 2, the primary parameter, which controls the release of Fe in the EOIF system is the current. As the magnitude of the current increases, the released Fe increases in the system. However, a large increase in the electrical current could result in Fe precipitation which leads to reduced Fe<sup>2+</sup> in solution. Therefore, changing the electrode geometry and material type was investigated as a first protocol to optimize the Fe release before controlling the electric current. Figures 4a, b show the measured concentration of Fe<sup>2+</sup> and Fe<sup>3+</sup> using various electrode geometries and materials (see Methods section for specific details). The results show that using Fe discs for both the anode and cathode leads to lower Fe<sup>2+</sup> concentration over time compared to using Fe plates or foils. This is because the Fe discs have smaller surfaces compared to the other geometries, so the surface available for the reactions is smaller, producing less Fe. The Fe foil electrodes result in a decreasing profile of Fe<sup>2+</sup> concentration over time. Since the foil is very thin, it conducts the electrical current very well. Therefore, the initial time it takes for the foil to release a large amount of Fe<sup>2+</sup> is due to its high efficiency in conducting the current. However, the produced Fe<sup>2+</sup> starts transforming into Fe(OH)<sub>2</sub> and precipitates because OH<sup>-</sup> production at the foil cathode is fast and efficient. Given that the reactor size is small and the electrodes are adjacent to each other, parasitic reactions such as the formation of Fe(OH)<sub>2</sub> can take place at the electrodes. However, the focus in this paper is on the primary reactions, and it should be emphasized that the final EOIF system would be engineered to reduce any secondary reactions, such as increasing the distance between the electrodes to prevent the reaction of the generated OH<sup>-</sup> with the Fe<sup>2+</sup> at the anode or vice versa.

In addition to studying the electrode geometry, different cathode materials were investigated to assess their cost-effectiveness and impact on the efficiency of Fe release. In the previous results, the Fe release was investigated in symmetrical electrochemical systems where the cathode and anode were made from Fe electrodes. Here, while keeping the same Fe plate anode, three different cathode materials were tested, including Fe plate, carbon bar, and titanium mixed metal oxides (Ti/MMO) mesh. The measurements show that using Ti/MMO as a cathode led to higher concentrations of Fe<sup>2+</sup> compared to the Fe plate and carbon cathodes. This indicates that Ti/MMO has higher electrochemical efficiency due to its mesh structure which allows for regulating the Fe release by forming a complex electric field domain with the anodic plate (i.e., both anode and cathode have different geometry, which results in a less effective electric field compared to using electrodes with same dimensions and geometry). The concentrations of Fe<sup>3+</sup> over time have the same values for the various electrodes (see Fig. 4). The carbon cathode shows an intermediate efficiency in terms of generating Fe<sup>2+</sup> over time. The concentration profile of Fe<sup>2+</sup> for the carbon-based cathode system lies between the Titanium-based and the Fe-plate cathode systems. Given the low cost of carbon-based materials, using carbon material as a cathode would be an optimum design in terms of cost and Fe release efficiency.

To investigate the efficiency of the Fe release as a function of the electric current, the current was varied from 40 to 220 mA using either a carbon or Ti/MMO cathode. Figure S5 shows that increasing the current from 40 to 100 mA increased the overall concentration of Fe<sup>2+</sup> for the carbon-based cathode system. The further increase to 220 mA led to a minimal increase in Fe generation compared to lower current values. Similar trends were observed while using a Ti/MMO cathode, as shown in Figure S6. This is due to the large and fast Fe generation at the anode. The rapid generation of Fe at larger currents makes it harder for the released Fe to have enough time to dissolve in the seawater and therefore Fe<sup>2+</sup> will have a minimum concentration. Alternatively, pulsed current and polarity reversal techniques<sup>80,81</sup> can be respectively used for manipulating the current and switching between

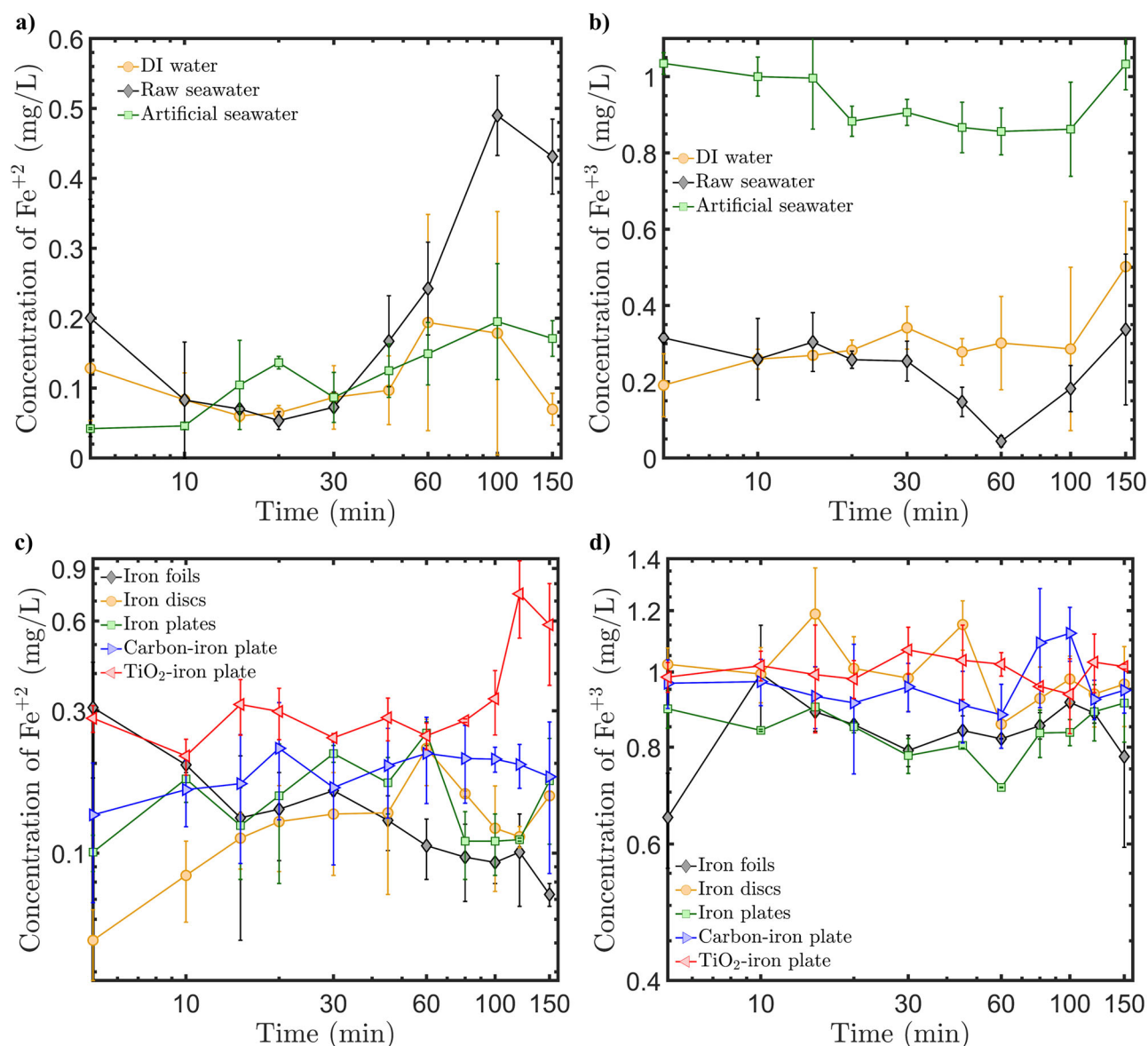


**Fig. 4 | Measured concentrations of the electrochemically released Fe forms as a function of time under 160 mA electrical current. a and b** Fe<sup>2+</sup> and Fe<sup>3+</sup> concentrations, respectively, for various electrodes, **c** Fe<sup>2+</sup> (solid lines) and Fe<sup>3+</sup> (dashed

lines) concentrations under current pulsing conditions, and **d** Fe<sup>2+</sup> (solid lines) and Fe<sup>3+</sup> (dashed lines) concentrations under polarity reversal conditions.

the electrodes (i.e., anode to cathode or vice versa) to regulate and maximize the Fe release and its bioavailability. Pulsed current is applied by switching the current on/off for different time cycles. Figure 4c shows that Fe<sup>2+</sup> production can be completely suppressed by pulsing the current every 10 min (i.e., 10 min ON followed by 10 min OFF) for either carbon- or titanium-based cathode systems. If the current is pulsed every 5 min, a slight generation of Fe<sup>2+</sup> was observed as a function of time. The Fe<sup>3+</sup> concentrations are larger for pulsed current every 5 min interval compared to 10 min interval. Overall, current pulsing over 5 min intervals using a Titanium-based cathode shows that the Fe<sup>2+</sup> concentration increases as the reaction time evolves while the Fe<sup>3+</sup> concentration decreases. This is attributed to providing enough time through pulsing for the Fe to dissolve into the seawater allowing more soluble Fe<sup>2+</sup> formation over insoluble Fe<sup>3+</sup>. Pulsing the current or other time-dependent current applications can be used to regulate the Fe release over time. The efficiency of the current pulsing technique needs to be better demonstrated in larger systems beyond 1-2 L reactors.

The polarity reversal approach is based on periodically switching the cathode to the anode and the anode to the cathode to regulate the

electrochemical kinetics. Figure 4d shows the Fe concentrations using the polarity reversal approach. Fe<sup>2+</sup> concentrations are higher when 10 min intervals of polarity reversal are applied. This is because a 10 min interval allows the Fe to be produced for 10 min and then the production is stopped for another 10 min giving more time for the Fe to dissolve in the seawater compared to the 5 min interval procedure. Furthermore, there is a point in time at which the Fe<sup>2+</sup> concentration reaches the maximum (~0.6 mg/L), and the Fe<sup>3+</sup> concentration is at a minimum (~0.9 mg/L). This point is at a 55 min mark of the 10 min polarity reversal curve using a Ti/MMO cathode. Optimization of the EOIF control parameters would be needed to take full advantage of the Fe bioavailability and regulate its release in the seawater.

## Discussion

### Solar-powered EOIF and techno-economic assessment

As shown in Fig. 2, the EOIF technology promotes sustainability where the input of electrical current can come from a renewable energy source such as solar power. To investigate the practicality of using solar energy to power the

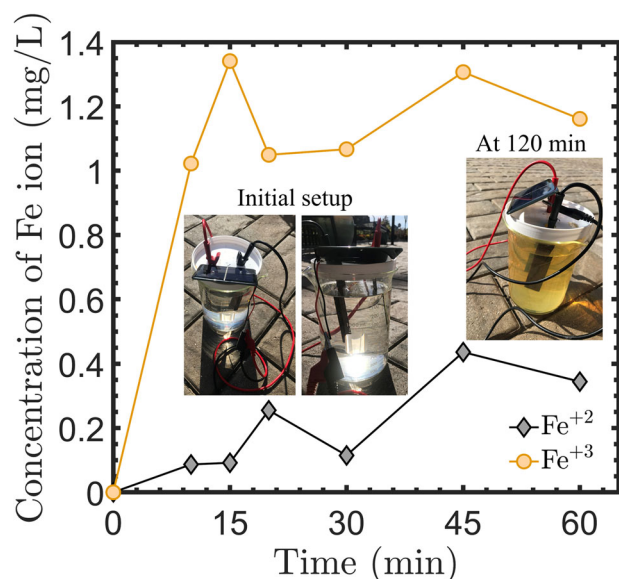


**Fig. 5 | Solar-powered EOIF.** Measured Fe<sup>2+</sup> and Fe<sup>3+</sup> concentrations when the current is supplied using a solar panel.

**Table 1 | Comparison of the financial costs of different mCDR technologies**

Technology	Financial cost (US\$/tons of CO <sub>2</sub> )
Ocean liming (OAE technology)	72–159 <sup>18</sup>
Electrochemical weathering (OAE technology)	14–190 <sup>18</sup>
Accelerated weathering of limestone (OAE technology)	10–40 <sup>18</sup>
Direct air capture (OAE technology)	100–1000 <sup>18</sup>
Traditional OIF via airplane delivery	7–415 <sup>84</sup>
Traditional OIF via ship delivery	9–1502 <sup>84</sup>
Self-operating solar-powered EOIF (combined OIF and OAE)	3.58–7.16

electrochemical reactions of the Fe release, small-scale experiments were performed as shown in Fig. 5. The solar-generated electrical current using a small panel (see Methods section for details) produced both Fe<sup>2+</sup> and Fe<sup>3+</sup> as expected. The results in Fig. 5 demonstrate that the concentration of the Fe (Fe<sup>2+</sup> and Fe<sup>3+</sup>) increases over time. A large presence of Fe<sup>3+</sup> was observed, that tuned the artificial seawater into a yellow color since this Fe form is insoluble. We also observed the generation and release of H<sub>2</sub> gas bubbles at the carbon cathode as shown in the recorded video (see the Supplementary Materials). The solar-harvested electrical current can be tuned and controlled using current control units or by adjusting the incident solar energy.

To demonstrate the cost feasibility of powering the EOIF platform using solar power, the financial cost of this technology was estimated and compared it to the other reported CDR approaches as shown in Table 1. First, the required amount of Fe to increase the ocean Fe concentration was set as the target of the techno-economic assessment based the experimentally reported values<sup>46</sup>. It is assumed that the ferrous Fe concentration (Fe<sup>2+</sup>) should be increased by 1 nM in seawater (i.e., an estimated value within a range to prevent supplying an unnecessarily large amount of Fe beyond the saturation growth limit of phytoplankton<sup>46</sup>). Assuming this 1 nM of Fe<sup>2+</sup> should be supplied over a surface area of 100 x 100 km (roughly one degree of latitude/longitude) and depth of 30 m, then the volume of the seawater will be  $3 \times 10^{11} \text{ m}^3$  or  $3 \times 10^{14} \text{ L}$ . The needed mass of ferrous Fe,  $m$ , is given as the product of the targeted supplied Fe concentration times the volume of the seawater such that  $m = 3 \times 10^5 \text{ mole}$  or 16.75 tons. Using Faraday's law

(i.e., Eq. 2), the amount of needed solar energy can be estimated in terms of the electrical current to supply  $3 \times 10^5 \text{ moles}$  of Fe<sup>2+</sup>. Assuming that the Fe amount is supplied over 5 years (i.e.,  $t = 15.77 \times 10^7 \text{ s}$ ), then the total needed current for the reactions, given that  $n = 2$  and  $F = 96,485 \text{ C/mole}$ , will be 367 A. This current can be obtained using a PV cells system of series panels of 20 kW where each panel can provide a current of ~6–8 A. Therefore, it is estimated that the platform requires about 70 connected solar panels of a total equivalent area of 1400 sq ft, which could cost about \$55,000 based on commercial online prices of solar panels. It should be noted that the needed 16.75 tons can be supplied by running several platforms at different locations in the ocean to complete fertilization in less than five years. These calculations show the feasibility of the EOIF process. The amount of the generated OH<sup>-</sup> during the five years process, and the usage of 367 A, can be determined using Eq. 1 as well. Given the time and current from the designed Fe release, the amount of released OH<sup>-</sup> will be around 10 tons or 2 nM over the targeted seawater volume. This amount will help in increasing and enhancing the alkalinity of the ocean. Thus, the invested \$55,000 in solar panels can provide 16.75 tons of Fe for OIF and 10 tons of OH<sup>-</sup> for OAE. The potential for mCDR is greater for OIF than OAE since the response and C growth and export efficiencies can be 1:1000 and higher via OIF compared to 1:1 efficiency via OAE<sup>17</sup>. Based on these efficiencies, the amount of removed CO<sub>2</sub> from the atmosphere can be estimated to be 16,760 tons based on the combined addition of 16.75 tons of Fe and 10 tons of OH<sup>-</sup> using the EOIF processes.

The estimated average price of iron is about ~\$90/ton. The total cost of the needed iron is about ~\$1,500. It can be assumed additional ~\$3,000 (double of the iron electrode's cost) will be needed to construct the EOIF platform and occupy it with the various equipment such as a power supply to control the current and carbon-based cathode. Thus, the total cost of the EOIF platform can be rounded up to \$60,000, which includes the cost of the solar panels, iron electrodes, platform frames, cathodes, and other equipment. This cost represents the price of materials and energy of the EOIF processes. For simplicity, the logistic cost is not considered in this analysis assuming a self-operating platform (i.e., in this case the cost of the logistic operations will mainly depend on the cost of the deployment of the EOIF platform in the ocean). Using the previously estimated amount of sequestered atmospheric CO<sub>2</sub> (16,760 tons) and the total cost of the EOIF platform (\$60,000), the estimated price of mCDR via EOIF is about \$3.58/tons of CO<sub>2</sub>. This techno-economic assessment shows that EOIF is a cost-effective approach compared to other mCDR methods where their financial cost is estimated to range between \$10–\$1000/tons of CO<sub>2</sub><sup>18,82,83</sup>. Even if the financial cost of EOIF is assumed to be doubled due to the logistics or any hidden effectiveness parameters (i.e., the cost becomes ~\$7.16/tons of CO<sub>2</sub> as an extreme case), the cost of the EOIF approach is still less than the other mCDR methods (<\$10/tons of CO<sub>2</sub>).

This feasibility analysis shows the effectiveness of the EOIF method. Previous experiments of OIF released about 1–3 ton of Fe over couple of weeks and batch size up to 300 km<sup>2,44</sup>. The previous theoretical estimation suggests that the EOIF approach releases almost 8 times the Fe and regulates it over longer periods of time (e.g., 5 years) instead of a couple of weeks. This allows for monitoring the biogeochemical response of the ecosystem over time, and also meets the marine demand of 10–100 ton of Fe<sup>7</sup>. In terms of cost, earlier experimental studies showed that the power requirement for electrochemical mCDR methods such as OAE is 1.8–2.3 MWh/tCO<sub>2</sub><sup>33,84–86</sup>. This is a large energy consumption, which could require building costly offshore wind turbines<sup>33</sup>. The high energy demands of traditional OAE techniques prevents effectively implementing and testing these techniques offshore. Overall, the EOIF system is a promising novel, sustainable, and cost-effective technology that provides a mCDR solution combining both OIF and OAE approaches.

### Demonstrating scalability of EOIF

The experimental results presented here are based on small-scale testing. It will be important to demonstrate the scalability of the proposed EOIF technology by testing larger systems. In larger systems, it is expected that the

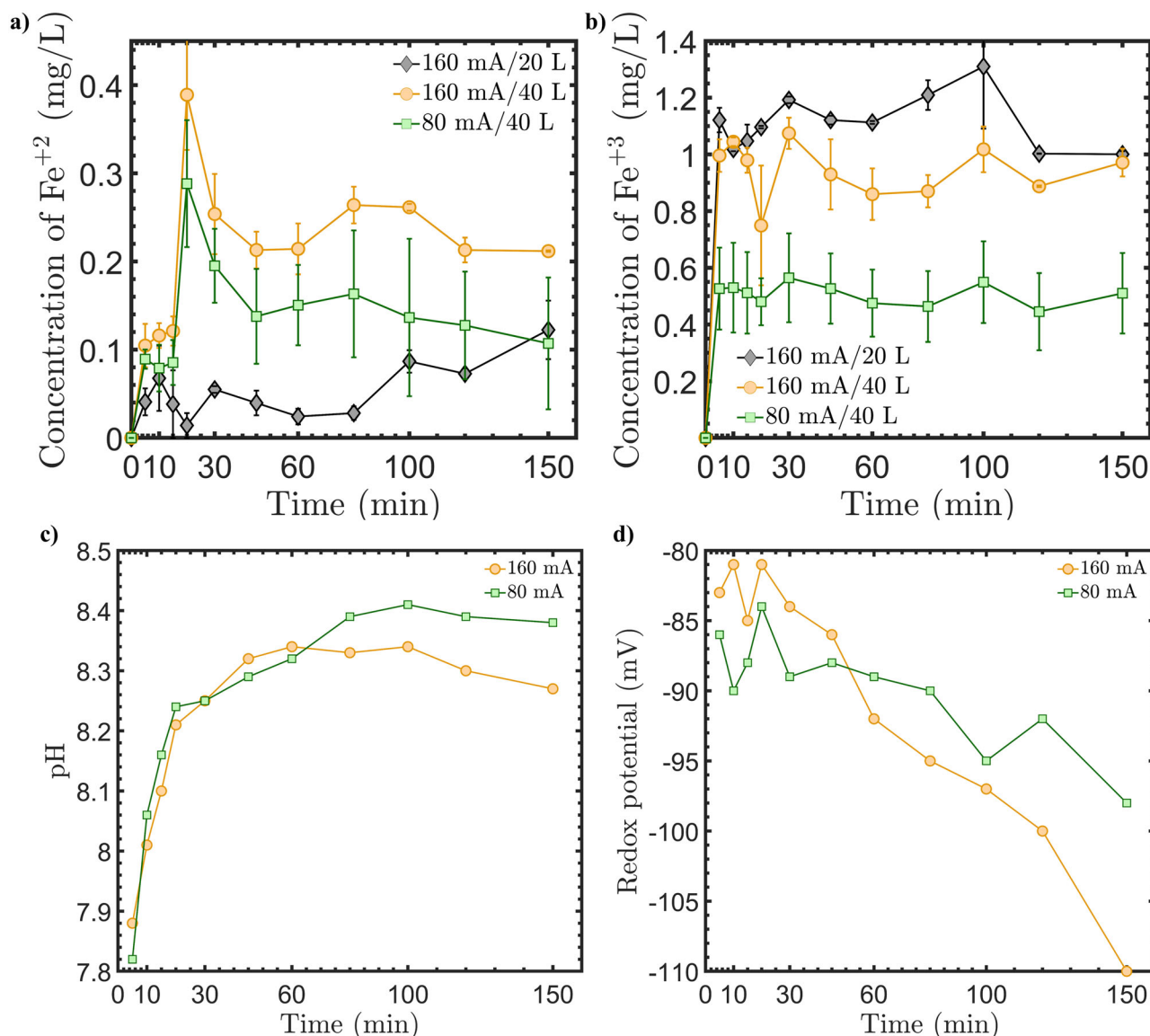


**Fig. 6 | Experimentally measured results during the electrochemical Fe release in large tanks.** **a** and **b** concentrations of  $\text{Fe}^{+2}$  and  $\text{Fe}^{+3}$ , respectively, as a function of time for various seawater tank sizes and currents, **c** pH evolution in 40 L seawater tank, and **d** the oxygen redox potential in the 40 L tank using 80 and 160 mA currents.

Fe concentrations become less (i.e., the same amount of released Fe mass at a given current but in larger seawater volume) and easier to control. Specifically, the  $\text{Fe}^{+3}$  concentration should be lower since the volume is increased, and natural ligands enhance  $\text{Fe}^{+2}$  solubility. To demonstrate that, the Fe release and pH variations were tested in larger tanks, as detailed in the Method section. Figure 6 shows the results for testing the EOIF system in 20 and 40 L tanks. First, the measured concentrations show that the  $\text{Fe}^{+2}$  is found to be less in the 20 L tank versus the 40 L tank under 160 mA, whereas the trend is the opposite for  $\text{Fe}^{+3}$  concentration. This supports our earlier observation about the competition and exchange between  $\text{Fe}^{+2}$  and  $\text{Fe}^{+3}$  forms in seawater. When the tank size is larger, the volume of seawater is larger and therefore the released  $\text{Fe}^{+2}$  will have sufficient vicinities to dissolve in the water without transferring into  $\text{Fe}^{+3}$ . Thus, the effective amount of the released  $\text{Fe}^{+2}$  can be increased and scaled with larger systems.

Next, an increase in Fe via EOIF can be achieved by tuning the applied current. Figure 6a shows that the  $\text{Fe}^{+2}$  concentration over time is proportional to the applied current for the same tank size (i.e., 40 L). As the current increases from 80 mA to 160 mA, an increase in the  $\text{Fe}^{+2}$  concentration was observed while maintaining the same concentration profile as a function of time for both currents. Furthermore, the  $\text{Fe}^{+3}$  concentration decreases by

almost 50% upon reducing the current from 160 mA to 80 mA. This is caused by the smaller electrochemical Fe flux using reduced potential (80 mA), which allows insoluble ferric Fe precipitation. The concentrations of  $\text{Fe}^{+3}$  and  $\text{Fe}^{+2}$  using the 20 and 40 L tanks represent promising scalability features of the EOIF technology. Finally, Fig. 6c, d show the time-dependent changes in the pH and redox potential of the seawater in the 40 L tank under 80 and 160 mA currents, which are relevant to alkalinity enhancement. The results show the pH of the seawater significantly increasing over time as expected for both currents by  $\sim 0.6$ . The redox potential also became more negative as time evolved indicating the formation of  $\text{OH}^-$  in the seawater. It should be highlighted that the pH under 80 mA is slightly higher than the pH under 160 mA, which can be justified by the possible consumption of  $\text{OH}^-$  to form  $\text{Fe}(\text{OH})_2$  in a secondary reaction as the current increases as previously discussed. Overall, the larger volume experiments validated the scalability of the EOIF technology toward achieving well-designed OIF and OAE processes.

#### Final remarks

EOIF technology represents a promising solution to increase the ocean capacity for  $\text{CO}_2$  removal and enhance primary production in the ocean



based by combining both OIF and OAE concepts, in addition to potentially allowing for hydrogen recovery from the ocean ( $H_2$  quantification was not tested here). The electrochemical release of Fe and  $OH^-$ , which are controlled by Faraday's law, demonstrate an engineered route to regulate the Fe release rate, its bioavailability, and the pH of the seawater. Unlike the traditional methods of OIF, the EOIF releases the Fe without the need to add any additional chemical compounds and offers the ability to regulate the release over time by controlling the applied current. Experimental results show that the electrochemical Fe release in natural raw seawater produces a concentration range of  $0.05 \text{ mg/L} < Fe^{+2} < 0.5 \text{ mg/L}$ , which can be lowered by either increasing the tank size or lowering the electric current. The detected  $Fe^{+2}$  in artificial seawater is almost 50% less than the detected concentration in natural seawater due to the transformation of  $Fe^{+2}$  into  $Fe^{+3}$  in artificial seawater (i.e.,  $Fe^{+3}$  concentration is almost 5 times higher in artificial seawater than natural seawater). This is attributed to the absence of natural organic matter and minerals in artificial seawater that help in stabilizing the electrochemically released Fe in natural seawater resulting in higher soluble  $Fe^{+2}$  concentration over the insoluble  $Fe^{+3}$ . Furthermore, the release of Fe in seawater can be controlled and optimized by varying the electrode materials and geometry. It was demonstrated that using a carbon-based cathode with a Fe plate anode can be a cost-effective option with an intermediate efficiency in terms of the released Fe form (i.e.,  $Fe^{+2}$  versus  $Fe^{+3}$ ). Using a Ti/MMO mesh cathode with an Fe plate anode result in maximum efficiency by producing the largest  $Fe^{+2}$  concentrations. The EOIF system offers several ways to control the Fe release and its form, such as current pulsing and polarity reversal. Our experiments revealed that  $Fe^{+2}$  production can be suppressed under certain electric current pulsing or polarity reversal conditions.

The applied current can be obtained from solar power. Solar-powered EOIF technology is a feasible and cost-effective solution to increasing the Fe concentration by either deploying several small EOIF platforms or a large platform to achieve the desired concentrations. In addition, the EOIF system demonstrates the potential to be scaled up, by adjusting the applied current and the volume and geometries. The key parameter that controls the Fe release is the magnitude of the applied electrical current. Therefore, lower  $Fe^{+3}$  concentrations can be optimized, leading to potentially higher bioavailable  $Fe^{+2}$ . In addition to the measured Fe concentration, the pH increased over 150 min by almost 0.6 for the 20 and 40 L tanks. The decreasing redox potential as a function of time indicates the release of  $OH^-$  in the system. While the EOIF technology represents a potential solution for OIF and OAE studies and deployments, additional investigations and field testing are required to achieve an optimized design, durability, and control systems for open ocean use. Comparing the bench scale experiments with the field studies is crucial for a reliable comparison between the EOIF technology and other OIF approaches at the larger scales. For example, the possible secondary reactions at the electrodes, such as the production of chloride gas and  $Fe(OH)_2$  formations should be studied. Specifically, integrated analysis of the scale-up parameters of the EOIF should be investigated in future work. This requires investigating the effect of the ocean mixing in both horizontal and vertical directions on the iron transport and the surface flux of  $CO_2$ . In addition, the mixing analysis can help in understanding the potential increase in the carbon export, and the potential risk of precipitation of Mg and Ca salts caused by localized high carbonate ion concentrations. Future studies can also help in quantifying the extent of OAE via EOIF in the field and the associated potential of the  $CO_2$  sequestration. Overall, the results are intended to bring EOIF to the attention of the scientific community as a potentially effective approach to reduce atmospheric  $CO_2$  and thus tackle climate change at larger scales.

## Methods

### Analytical and testing methods

During all tests, the  $Fe^{+2}$  and  $Fe^{+3}$  concentrations were quantified (Note: only the dissolved forms of iron were measured). All tests were performed at room conditions (i.e.,  $25^\circ C$  and 1 atm). Batch experiments were carried out in 1 and 2 L beakers. Large tests (i.e., 20 and 40 L) were in 40 L plastic tanks.

Analysis of  $Fe^{+2}$  and  $Fe^{+3}$  was determined by UV-VIS spectrophotometer (SHIMADZU UV-1800) at 510 nm wavelength, using the 1–10 phenanthroline analytical method<sup>87</sup>. To quantify the total dissolved Fe, a sample of 0.5 mL taken from the beaker was filtered by a 0.2-micron filter, then 0.25 mL of 10% hydroxylamine hydrochloride solution was added to reduce the dissolved Fe to  $Fe^{+2}$ . 1 mL of acetic acid buffer solution (20 g of ammonium acetate added to 25 mL of acetic acid in 100 mL of water) was added to adjust the pH from 3 to 5, and an addition of 1 mL of the 1–10 phenanthroline monohydrate (1 g/L) was added consecutively to the sample. The same procedure is followed to determine the concentration of  $Fe^{+2}$  using UV-VIS spectrophotometer at wavelength 510 nm except that no hydroxylamine hydrochloride was added. Finally, the concentration of  $Fe^{+3}$  was determined by taking the difference between the total dissolved Fe and  $Fe^{+2}$  concentrations.

The calibrations of the  $Fe^{+2}$  and  $Fe^{+3}$  concentrations performed by the spectrophotometer are shown in Figure S1 and Figure S2. Continuous measurements of pH and oxygen reduction potential (ORP) at top of the reactor were carried out using portable electrochemical pH probe meters with an estimated error of 0.1 in the pH values. At the beginning of each experiment, the testing beakers/tanks were washed and brushed several times with DI water and sulfuric acid (10% by weight) to remove any contaminants of the surface. All collected samples were filtered using 0.2-micron membranes (13 mm syringe filters with Millex-LG hydrophilic PTFE membrane before analyzing the Fe concentrations. All experiments of the figures in the main manuscript were repeated three times to obtain proper averaging and estimate the potential errors. The electrical current was applied across the electrodes using an Agilent E3612A DC power supply by setting it to constant current output. The solar-powered experiment was carried out using a 60 mm x 90 mm solar panel of 1 V and 400–500 mA outputs.

### Materials for testing

Solid Fe electrodes in different shapes were tested ranging from a plate, disc, and foil to investigate the effect of electrode geometry on the Fe release in seawater. The plate electrode is 19.05 mm wide x 101.6 mm long and weighs about 12 grams. The disc Fe electrode is 24.26 mm in diameter with 99.9% purity. The foil electrode was cut from a  $0.1 \times 100 \times 1000$  mm Fe sheet with 99.995% purity. A piece was cut that has a width and length equal to the plate electrode dimensions. For the carbon electrode, carbon bars were used with dimensions of  $100 \times 20 \times 5$  mm made by Eisco labs. Ti/MMO electrode consists of  $IrO_2$  and  $Ta_2O_5$  coating on Titanium, with a diameter of 2.9 cm and 2 mm in thickness with a purity of 99%.

Artificial seawater electrolyte was prepared in the lab. The chemical compositions of the prepared artificial seawater samples are detailed in Table S1. These chemical compositions are determined based on previous work<sup>88</sup>. The chemical minerals and compositions were added to DI water to synthesize the artificial seawater samples. The reported experiments in this manuscript are based on Sample 2 composition shown in Table S1 except for Figure S3 where both artificial seawaters from Sample 1 and 2 were tested and compared. The natural unfiltered and filtered seawater samples were collected at Cape Code shore in Massachusetts, United States of America.

### Data availability

Additional data supporting the analyses and results of this study are available in the Supplementary Information. Additional generated data are also available from the corresponding author upon request.

Received: 6 August 2023; Accepted: 22 April 2024;

Published online: 14 May 2024

## References

1. Büntgen, U. et al. Recent European drought extremes beyond Common Era background variability. *Nat. Geosci.* **14**, 190–196 (2021).
2. Magnan, A. K. et al. Estimating the global risk of anthropogenic climate change. *Nat. Clim. Change* **11**, 879–885 (2021).

3. Woolway, R. I. et al. Global lake responses to climate change. *Nat. Rev. Earth Environ.* **1**, 388–403 (2020).
4. Jansson, J. K. & Hofmockel, K. S. Soil microbiomes and climate change. *Nat. Rev. Microbiol.* **18**, 35–46 (2020).
5. UNFCCC. Paris Agreement to the United Nations Framework Convention on Climate Change. (12 December 2015).
6. NRC. Climate intervention: Carbon dioxide removal and reliable sequestration. Washington, DC: The National Academies Press (2015).
7. Buesseler, K. et al. Ocean iron fertilization: assessing its potential as a climate solution *ExOIS*, <https://oceaniron.org/our-plan/> (2022).
8. Mac Dowell, N., Fennell, P. S., Shah, N. & Maitland, G. C. The role of CO<sub>2</sub> capture and utilization in mitigating climate change. *Nat. Clim. Change* **7**, 243–249 (2017).
9. Breyer, C. Low-cost solar power enables a sustainable energy industry system. *Proc. Natl. Acad. Sci. USA* **118**, <https://doi.org/10.1073/pnas.2116940118> (2021).
10. Hoehne, C. G. & Chester, M. V. Optimizing plug-in electric vehicle and vehicle-to-grid charge scheduling to minimize carbon emissions. *Energy* **115**, 646–657 (2016).
11. Álvarez Fernández, R. A more realistic approach to electric vehicle contribution to greenhouse gas emissions in the city. *J. Clean. Prod.* **172**, 949–959 (2018).
12. Wilberforce, T., Baroutaji, A., Soudan, B., Al-Alami, A. H. & Olabi, A. G. Outlook of carbon capture technology and challenges. *Sci. Total Environ.* **657**, 56–72 (2019).
13. Hills, T., Leeson, D., Florin, N. & Fennell, P. Carbon Capture in the Cement Industry: Technologies, Progress, and Retrofitting. *Environ. Sci. Technol.* **50**, 368–377 (2016).
14. Berrill, P., Wilson, E. J. H., Reyna, J. L., Fontanini, A. D. & Hertwich, E. G. Decarbonization pathways for the residential sector in the United States. *Nat. Clim. Change* **12**, 712–718 (2022).
15. Papadis, E. & Tsatsaronis, G. Challenges in the decarbonization of the energy sector. *Energy* **205**, <https://doi.org/10.1016/j.energy.2020.118025> (2020).
16. Tian, Y. et al. Promises and Challenges of Next-Generation “Beyond Li-ion” Batteries for Electric Vehicles and Grid Decarbonization. *Chem. Rev.* **121**, 1623–1669 (2021).
17. National Academies of Sciences, E. a. M. Negative emissions technologies and reliable sequestration: A research agenda. The National Academies Press, Washington, DC, <https://doi.org/10.17226/25259> (2019).
18. Renforth, P. & Henderson, G. Assessing ocean alkalinity for carbon sequestration. *Rev. Geophys.* **55**, 636–674 (2017).
19. Archer, D., Kheshgi, H. & Maier-Reimer, E. Multiple timescales for neutralization of fossil fuel CO<sub>2</sub>. *Geophys. Res. Lett.* **24**, 405–408 (1997).
20. Siegenthaler, U. & Sarmiento, J. L. Atmospheric carbon dioxide and the ocean. *Nature* **365**, 119–125 (1993).
21. National Academies of Sciences, E., and Medicine. A Research Strategy for Ocean-based Carbon Dioxide Removal and Sequestration., (The National Academies Press, Washington, DC, 2022).
22. Board, O. S. & Council, N. R. *Climate intervention: Reflecting sunlight to cool earth*. (National Academies Press, 2015).
23. Seddon, N., Turner, B., Berry, P., Chausson, A. & Girardin, C. A. J. Grounding nature-based climate solutions in sound biodiversity science. *Nat. Clim. Change* **9**, 84–87 (2019).
24. Amelung, W. et al. Towards a global-scale soil climate mitigation strategy. *Nat. Commun.* **11**, 5427 (2020).
25. Cook-Patton, S. C. et al. Protect, manage and then restore lands for climate mitigation. *Nat. Clim. Change* **11**, 1027–1034 (2021).
26. Kantzas, E. P. et al. Substantial carbon drawdown potential from enhanced rock weathering in the United Kingdom. *Nat. Geosci.* **15**, 382–389 (2022).
27. Watson, A. J. et al. Revised estimates of ocean-atmosphere CO<sub>2</sub> flux are consistent with ocean carbon inventory. *Nat. Commun.* **11**, 4422 (2020).
28. Berner, R. A. The Rise of Plants and Their Effect on Weathering and Atmospheric CO<sub>2</sub>. *Science* **276**, 544–546 (1997).
29. O’Mara, N. A. & Dunne, J. P. Hot Spots of Carbon and Alkalinity Cycling in the Coastal Oceans. *Sci. Rep.* **9**, 4434 (2019).
30. Bach, L. T., Gill, S. J., Rickaby, R. E. M., Gore, S. & Renforth, P. CO<sub>2</sub> Removal With Enhanced Weathering and Ocean Alkalinity Enhancement: Potential Risks and Co-benefits for Marine Pelagic Ecosystems. *Frontiers in Climate* **1**, <https://doi.org/10.3389/fclim.2019.00007> (2019).
31. Doney, S. C., Busch, D. S., Cooley, S. R. & Kroeker, K. J. The Impacts of Ocean Acidification on Marine Ecosystems and Reliant Human Communities. *Annu. Rev. Environ. Resour.* **45**, 83–112 (2020).
32. Society, R. Ocean acidification due to increasing atmospheric carbon dioxide. *Policy Doc. 12/05, R. Soc., London* (2005).
33. Wang, H. et al. Simulated Impact of Ocean Alkalinity Enhancement on Atmospheric CO<sub>2</sub> Removal in the Bering Sea. *Earth’s Future* **11**, <https://doi.org/10.1029/2022ef002816> (2023).
34. Zeebe R. E., W.-G D. *CO<sub>2</sub> in Seawater: Equilibrium, Kinetics, Isotopes*. (Elsevier, 2001).
35. Boyd, P. W. et al. A mesoscale phytoplankton bloom in the polar Southern Ocean stimulated by iron fertilization. *Nature* **407**, 695–702 (2000).
36. Babakhani, P. et al. Potential use of engineered nanoparticles in ocean fertilization for large-scale atmospheric carbon dioxide removal. *Nat. Nanotechnol.* **17**, 1342–1351 (2022).
37. Lauderdale, J. M., Braakman, R., Forget, G., Dutkiewicz, S. & Follows, M. J. Microbial feedbacks optimize ocean iron availability. *Proc. Natl Acad. Sci. USA* **117**, 4842–4849 (2020).
38. Boyd, P. W. et al. Mesoscale iron enrichment experiments 1993-2005: synthesis and future directions. *Science* **315**, 612–617 (2007).
39. Satak, R., Camadro, J. M. & Lesuisse, E. Iron Uptake Mechanisms in Marine Phytoplankton. *Front Microbiol* **11**, 566691 (2020).
40. Rouxel, O. J., Bekker, A. & Edwards, K. J. Iron isotope constraints on the Archean and Paleoproterozoic ocean redox state. *Science* **307**, 1088–1091 (2005).
41. Blain, S. et al. Effect of natural iron fertilization on carbon sequestration in the Southern Ocean. *Nature* **446**, 1070–1074 (2007).
42. Mazzotta, M. G., Mcllvain, M. R. & Saito, M. A. Characterization of the Fe metalloproteome of a ubiquitous marine heterotroph, *Pseudoalteromonas* (BB2-AT2): multiple bacterioferritin copies enable significant Fe storage. *Metallomics* **12**, 654–667 (2020).
43. Emerson, D. Biogenic Iron Dust: A Novel Approach to Ocean Iron Fertilization as a Means of Large Scale Removal of Carbon Dioxide From the Atmosphere. *Front. Marine Sci.* **6**, <https://doi.org/10.3389/fmars.2019.00022> (2019).
44. Yoon, J.-E. et al. Reviews and syntheses: Ocean iron fertilization experiments – past, present, and future looking to a future Korean Iron Fertilization Experiment in the Southern Ocean (KIFES) project. *Biogeosciences* **15**, 5847–5889 (2018).
45. Williamson, P. et al. Ocean fertilization for geoengineering: A review of effectiveness, environmental impacts and emerging governance. *Process Saf. Environ. Prot.* **90**, 475–488 (2012).
46. Sunda, W. G. & Huntsman, S. A. Interrelated influence of iron, light and cell size on marine phytoplankton growth. *Nature* **390**, 389–392 (1997).
47. Martin, J. H. & Fitzwater, S. E. Iron deficiency limits phytoplankton growth in the north-east Pacific subarctic. *Nature* **331**, 341–343 (1988).
48. Siegel, D. A., DeVries, T., Doney, S. C. & Bell, T. Assessing the sequestration time scales of some ocean-based carbon dioxide reduction strategies. *Environ. Res. Lett.* **16**, <https://doi.org/10.1088/1748-9326/ac0be0> (2021).

49. Iversen, M. H. Carbon Export in the Ocean: A Biologist's Perspective. *Ann. Rev. Mar. Sci.* **15**, 357–381 (2023).
50. Carvalho, A. C. O., Kerr, R., Mendes, C. R. B., Azevedo, J. L. L. & Tavano, V. M. Phytoplankton strengthen CO<sub>2</sub> uptake in the South Atlantic Ocean. *Progr. Oceanogr.* **190**, <https://doi.org/10.1016/j.pcean.2020.102476> (2021).
51. Buesseler, K. O. et al. Environment. Ocean iron fertilization—moving forward in a sea of uncertainty. *Science* **319**, 162 (2008).
52. Marañón E. Phytoplankton Size Structure. *Academic Press Encyclopedia of Ocean Sciences (Second Edition)*, 445–452, <https://doi.org/10.1016/B978-012374473-9.00661-5> (2008).
53. Joos, F., Sarmiento, J. L. & Siegenthaler, U. Estimates of the effect of Southern Ocean iron fertilization on atmospheric CO<sub>2</sub> concentrations. *Nature* **349**, 772–775 (1991).
54. Pollard, R. T. et al. Southern Ocean deep-water carbon export enhanced by natural iron fertilization. *Nature* **457**, 577–580 (2009).
55. de Baar, H. J. W. Synthesis of iron fertilization experiments: From the Iron Age in the Age of Enlightenment. *J. Geophys. Res.* **110**, <https://doi.org/10.1029/2004jc002601> (2005).
56. Nishioka, J. et al. Size-fractionated iron distributions and iron-limitation processes in the subarctic NW Pacific. *Geophys. Res. Lett.* **30**, <https://doi.org/10.1029/2002gl016853> (2003).
57. Shaked, Y. & Lis, H. Disassembling iron availability to phytoplankton. *Front Microbiol* **3**, 123 (2012).
58. Lakshmanan, D., Clifford, D. A. & Samanta, G. Ferrous and ferric ion generation during iron electrocoagulation. *Environ. Sci. Technol.* **43**, 3853–3859 (2009).
59. Kim, S. et al. Asymmetric chloride-mediated electrochemical process for CO<sub>2</sub> removal from oceanwater. *Energy Environ. Sci.* <https://doi.org/10.1039/d2ee03804h> (2023).
60. Yan, L., Bao, J., Shao, Y. & Wang, W. An Electrochemical Hydrogen-Looping System for Low-Cost CO<sub>2</sub> Capture from Seawater. *ACS Energy Lett.* **7**, 1947–1952 (2022).
61. Rau, G. H. et al. Direct electrolytic dissolution of silicate minerals for air CO<sub>2</sub> mitigation and carbon-negative H<sub>2</sub> production. *Proc. Natl Acad. Sci. USA* **110**, 10095–10100 (2013).
62. Sharifian, R., Boer, L., Wagterveld, R. M. & Vermaas, D. A. Oceanic carbon capture through electrochemically induced in situ carbonate mineralization using bipolar membrane. *Chem. Engin. J.* **438**, <https://doi.org/10.1016/j.cej.2022.135326> (2022).
63. Oloye, O. & O'Mullane, A. P. Electrochemical Capture and Storage of CO<sub>2</sub> as Calcium Carbonate. *ChemSusChem* **14**, 1767–1775 (2021).
64. Sharifian, R., Wagterveld, R. M., Digdaya, I. A., Xiang, C. & Vermaas, D. A. Electrochemical carbon dioxide capture to close the carbon cycle. *Energy Environ. Sci.* **14**, 781–814 (2021).
65. Yang, N. et al. Iron electrolysis-assisted peroxydisulfate chemical oxidation for the remediation of chlorophenol-contaminated groundwater. *J. Chem. Technol. Biotechnol.* **91**, 938–947 (2016).
66. Yuan, S., Liao, P. & Alshawabkeh, A. N. Electrolytic manipulation of persulfate reactivity by iron electrodes for trichloroethylene degradation in groundwater. *Environ. Sci. Technol.* **48**, 656–663 (2014).
67. Baek, K., Ciblak, A., Mao, X., Kim, E. J. & Alshawabkeh, A. Iron anode mediated transformation of selenate in sand columns. *Water Res* **47**, 6538–6545 (2013).
68. Sarahney, H., Mao, X. & Alshawabkeh, A. N. Role of Iron Anode Oxidation on Transformation of Chromium by Electrolysis. *Electrochim. Acta* **86**, 96–101 (2012).
69. Mao, X., Baek, K. & Alshawabkeh, A. N. Iron Electrocoagulation with Enhanced Cathodic Reduction for the Removal of Aqueous Contaminant Mixtures. *Environ. Eng. Manag. J.* **14**, 2905–2911 (2015).
70. Tong, M. et al. Electrochemically induced oxidative precipitation of Fe(II) for As(III) oxidation and removal in synthetic groundwater. *Environ. Sci. Technol.* **48**, 5145–5153 (2014).
71. Zhao, Y., Hojabri, S., Sarrouf, S. & Alshawabkeh, A. N. Electrogeneration of H<sub>2</sub>O<sub>2</sub> by graphite felt double coated with polytetrafluoroethylene and polydimethylsiloxane. *J. Environ. Chem. Engineer.* **10**, <https://doi.org/10.1016/j.jece.2022.108024> (2022).
72. Compton, P., Dehkordi, N. R., Sarrouf, S., Ehsan, M. F. & Alshawabkeh, A. N. In-situ electrochemical synthesis of H<sub>2</sub>O<sub>2</sub> for p-nitrophenol degradation utilizing a flow-through three-dimensional activated carbon cathode with regeneration capabilities. *Electrochimica Acta* **441**, <https://doi.org/10.1016/j.electacta.2022.141798> (2023).
73. Matheson, L. J. & Tratnyek, P. G. Reductive dehalogenation of chlorinated methanes by iron metal. *Environ. Sci. Technol.* **28**, 2045–2053 (1994).
74. Huang, C.-H. et al. Effect of Chloride Ions on Electro-Coagulation to Treat Industrial Wastewater Containing Cu and Ni. *Sustainability* **12**, <https://doi.org/10.3390/su12187693> (2020).
75. Kuang, Y. et al. Solar-driven, highly sustained splitting of seawater into hydrogen and oxygen fuels. *Proc. Natl Acad. Sci. USA* **116**, 6624–6629 (2019).
76. Mi, Z., Zhang, X. & Chen, C. Iron release in drinking water distribution systems by feeding desalinated seawater: characteristics and control. *Desalination Water Treat.* **57**, 9728–9735 (2015).
77. Yan, B. A. Z. B. and 楊, 宗興 and Pan, X. Concentration and species of dissolved iron in waters in Sanjiang plain, China. 183–194 (2010).
78. Yuan, Y., Jiang, M., Zhu, X., Yu, H. & Otte, M. L. Interactions between Fe and light strongly affect phytoplankton communities in a eutrophic lake. *Ecological Indicators* **126**, <https://doi.org/10.1016/j.ecolind.2021.107664> (2021).
79. Morel, F. M. M., Kustka, A. B. & Shaked, Y. The role of unchelated Fe in the iron nutrition of phytoplankton. *Limnol. Oceanogr.* **53**, 400–404 (2008).
80. Zhou, W. et al. Efficient H<sub>2</sub>O<sub>2</sub> electrogeneration at graphite felt modified via electrode polarity reversal: Utilization for organic pollutants degradation. *Chem. Eng. J.* **364**, 428–439 (2019).
81. Zhou, W. et al. Highly efficient H<sub>2</sub>O<sub>2</sub> electrogeneration from O<sub>2</sub> reduction by pulsed current: Facilitated release of H<sub>2</sub>O<sub>2</sub> from porous cathode to bulk. *J. Taiwan Inst. Chem. Eng.* **83**, 59–63 (2018).
82. Strefler, J., Amann, T., Bauer, N., Kriegl, E. & Hartmann, J. Potential and costs of carbon dioxide removal by enhanced weathering of rocks. *Environ. Res. Lett.* **13**, <https://doi.org/10.1088/1748-9326/aaa9c4> (2018).
83. Emerson, D., Michaud, A., Archer, S., Sofen, L. & Twining, B. A cost model for ocean iron fertilization as a means of carbon dioxide removal that compares 2ship-and aerial-based delivery, and estimates verification costs. <https://doi.org/10.31223/x5wm12> (2023).
84. Eisaman, M. D. et al. Indirect ocean capture of atmospheric CO<sub>2</sub>: Part II. Understanding the cost of negative emissions. *Int. J. Greenh. Gas. Control* **70**, 254–261 (2018).
85. de Lannoy, C.-F. et al. Indirect ocean capture of atmospheric CO<sub>2</sub>: Part I. Prototype of a negative emissions technology. *Int. J. Greenh. Gas. Control* **70**, 243–253 (2018).
86. Eisaman, M. D. Negative Emissions Technologies: The Tradeoffs of Air-Capture Economics. *Joule* **4**, 516–520 (2020).
87. Komadel, P. & Stucki, J. W. Quantitative assay of minerals for Fe<sup>2+</sup> and Fe<sup>3+</sup> using 1, 10-phenanthroline: III. A rapid photochemical method. *Clays Clay Miner.* **36**, 379–381 (1988).
88. Sverdrup, H. U., Johnson, M. W. & Fleming, R. H. *The Oceans Their Physics, Chemistry, and General Biology*. (Prentice-Hall, Inc., 1942).

## Acknowledgements

The concept was developed from prior work on electrolysis by iron anodes for water treatment that was supported by the Superfund Research Program of the National Institute of Environmental Health Sciences (NIEHS), National Institutes of Health (NIH; grant number P42ES017198). The authors also

acknowledge WHOI-Northeastern joint seed funds provided by Northeastern to support this work.

### Author contributions

A.T., K.B. and A.N.A. conceived the study. A.T. and A.N.A. designed the study. A.T. and S.S. performed the experimental measurements and the Fe analysis. A.T. wrote the first draft of the manuscript with input from all authors. A.T., S.S., M.F.E., K.B., and A.N.A. reviewed and edited the manuscript. A.N.A. acquired the funding and led the supervision of this work.

### Competing interests

The authors declare no competing interests.

### Additional information

**Supplementary information** The online version contains supplementary material available at

<https://doi.org/10.1038/s44183-024-00064-8>.

**Correspondence** and requests for materials should be addressed to Akram N. Alshwabkeh.

**Reprints and permissions information** is available at <http://www.nature.com/reprints>

**Publisher's note** Springer Nature remains neutral with regard to jurisdictional claims in published maps and institutional affiliations.

**Open Access** This article is licensed under a Creative Commons Attribution 4.0 International License, which permits use, sharing, adaptation, distribution and reproduction in any medium or format, as long as you give appropriate credit to the original author(s) and the source, provide a link to the Creative Commons licence, and indicate if changes were made. The images or other third party material in this article are included in the article's Creative Commons licence, unless indicated otherwise in a credit line to the material. If material is not included in the article's Creative Commons licence and your intended use is not permitted by statutory regulation or exceeds the permitted use, you will need to obtain permission directly from the copyright holder. To view a copy of this licence, visit <http://creativecommons.org/licenses/by/4.0/>.

© The Author(s) 2024